Surfaces and Interfaces 32 (2022) 102154

Contents lists available at ScienceDirect

Surfaces and Interfaces

journal homepage: www.sciencedirect.com/journal/surfaces-and-interfaces

# Experimental and numerical studies of polyamide 11 and 12 surfaces modified by atmospheric pressure plasma treatment

M. Bahrami [a,*], D. Lavayen-Farfan [b], M.A. Martínez [a], J. Abenojar [a,c]

[a] Materials Science and Engineering Department, In-service material performance group, Álvaro Alonso Barba Institute of Chemistry and Materials Technology, University Carlos III of Madrid, Avda. Universidad, 30, 28911 Leganés, Madrid, Spain
[b] Department of Mechanical Engineering, University Carlos III of Madrid, Avda. Universidad, 30, 28911 Leganés, Spain
[c] Mechanical Engineering Department, Universidad Pontificia Comillas, Alberto Aguilera, 23, 28015 Madrid, Spain

ARTICLE INFO

*Keywords:*
Polyamide
APPT
Adhesion strength, CZM, Finite element model
Surface energy

ABSTRACT

Polyamide 11 and 12 (PA11 and PA12) have been applicable in various industries, including automotive, oil and gas, and sporting goods, over the past 70 years. Although they have good dyeability, their adhesion to other materials is limited due to relatively poor surface properties, which can be promoted by good wettability and high surface energy. This study aims to improve the surface properties of PA11 and PA12 by employing the advanced method of Atmospheric Pressure Plasma Torch (APPT) treatment. In this regard, the adhesion strengths of four commercially available adhesives were evaluated with the pull-off test on PAs plates before and after APPT treatment. The numerical simulation of this test was carried out in commercial finite element software using a cohesive zone model (CZM) to predict the fracture of adhesively bonded joints. Moreover, the modified PAs were analyzed using XPS, DSC, ATR-FTIR, optical profilometer and surface energy measurement. The results indicated that the surface properties, including wettability, polar surface energy and adhesion bonding, improved by employing the plasma treatment on PAs surfaces. The numerical simulation outcomes showed that the pull-off test might be a viable alternative to determine the CZM laws for fracture mode I.

## 1. Introduction

After the discovery of polyamides (PAs) by Carothers in 1940 [1], they have received tremendous interest in various industries such as automotive, textile, sports, and oil and gas due to their excellent properties like mechanical strength, chemical resistance, ease of processing, high melting point and low permeability for oxygen [2,3]. Despite their satisfactory bulk properties, PAs surface typically possesses poor surface properties, including low surface energy, poor adhesion and insufficient wettability, leading to processing problems in various applications, especially when coated, printed or joined with other materials [3,4]. These shortcomings are mainly caused by low reactivity of the surface, e.g., absence or dearth of reactive functional groups on the surface.

Along with PA6 and PA66, the most applicable polyamides (90% of the world's consumption of PAs [5]), PA11 and 12, which are semi-crystalline polyamides, have attracted increasing interest over the past 70 years. PA12 is an oil-based engineering thermoplastic, while the PA11 is a bio-based polyamide synthesized from renewable resources (e.g., castor plants) with a lower carbon footprint [6,7].

Fig. 1 compares the PA11 and PA12 with polypropylene (PP) and polyethylene (PE) from a structural point of view. The PP and PE, generally polyolefins, which are the most widely used commercial polymers, are made of nonpolar covalent bonds of C—C and C—H, resulting in poor surface adhesion properties [8,9]. They resist being wetted by adhesives due to the low surface energy. In other words, PP and PE with a surface energy of 31 mJ/m$^2$ [10] do not make enough intimate contact with adhesives, coatings or other more polar polymers which is necessary for good bonding. On the other side, polyamides are made up of amide groups (linkage of amine with carboxylic acid group) that interact along linear alkane chains [11]. The hydrogen bonding between amide groups of neighboring chains plays a major role in the surface properties of polyamides. Although polyamides like polyolefins are categorized as low surface energy (LSE) plastics, their higher reported surface energy than polyolefins (35–53 mJ/m$^2$ [10,12-14]) is more favorable in terms of surface properties.

From the adhesion point of view, the adhesion of PAs to more polar polymers or other substrates is a challenging issue that should be solved before final application. The dominant parameters to promote adhesion

* Corresponding author.
*E-mail address:* mbahrami@ing.uc3m.es (M. Bahrami).

https://doi.org/10.1016/j.surfin.2022.102154
Received 9 March 2022; Received in revised form 6 June 2022; Accepted 25 June 2022
Available online 1 July 2022

properties are high surface energy, a large contact surface area, and good wettability [15,16]. Consequently, several attempts have been made to improve the surface properties of PAs. Among the numerous techniques, plasma treatments have become progressively popular. To cite some examples of research on this matter, Mandolfino et al. [17] treated PA6 and PA6.6 surfaces with a low-pressure plasma to increase wettability properties and shear strength of the bonded joints with PAs. The plasma treatment increased the oxygen-containing polar groups on both polyamides, led to wettability and hydrophilicity improvement of the surface. A low concentration of active species, which results in longer exposure times, is one of the disadvantages of the low-pressure plasma technique, limiting its use commercially and industrially [3]. Hnilica et al. [18] achieved a significant increase in wettability of PA12 films by microwave plasma jet, which caused chemical and morphological changes on the surface. In another study, Károly et al. [4] modified the surface of PA6 with cold plasma treatment. Due to the formation of oxygen-containing functionalities on the surface, the surface energy, wettability, and adhesion shear strength of PA6 improved. Vlasta et al. [3] could decrease the water contact angle of the PA6 foils to less than half of the initial value by employing plasma treatment with two different discharge sources. Furthermore, the peel resistance improved 19% after 2 s diffuse coplanar surface barrier discharge (DCSBD) plasma treatment. In various papers [19–21], Geo and his team investigated the effect of atmospheric pressure plasma jet treatment on the PA6 films. In this regard, the plasma-treated samples had higher roughness, hydrophilic surface groups and higher T-peel strength. Also, adding a small amount of $O_2$ to the $CF_4$ and He as plasma gasses improved surface properties as well. Moreover, the presence of moisture and environmental humidity facilitated the effectiveness of plasma treatment [22].

The plasma treatment techniques that polymer is exposed to reactive gaseous particles and radiation from gaseous plasma present noteworthy advantages in the modification of polymeric surfaces (1) treatment confined to a region only several molecular layers deep without affecting the bulk properties, (2) nontoxic, dry, and environmentally friendly, (3) applicable for a wide range of materials, (4) easy and fast process with controllable parameters, (5) capable of surface morphology and roughness modification by etching effect, to name but a few [23–25].

In this study, the Atmospheric Pressure Plasma Torch (APPT) treatment was applied on the surface of polyamide 11 and 12 in order to modify the surface properties and improve their adhesion properties. In the APPT treatment, which is a cold plasma technique, a compressed air flux is expelled through a nozzle after ionization by the action of two electrodes. This process has been widely used in adhesives, coatings and sealants fields because it usually forms hydroxyl and amine functional groups or polar oxygen-containing groups (–COOH, –OH), thus promoting the surface energy and wettability and enhancing the interaction with the adhesive [26–28].

The adhesion bonding strength of treated surfaces can be evaluated experimentally through different methods such as the pull-off test. Nowadays, numerical simulations are considered trending tools to predict or facilitate experimental studies. In the present study, to apply the results of the pull-off test to further engineering problems and applications, a numerical model of the test was developed. The numerical model aimed to use these results as the cohesive zone laws for finite element simulations. The cohesive zone model (CZM), first proposed by Dugdale [29] and Barenblatt [30], is a damage model used in fracture mechanics that captures the overall behavior of the crack interface and incorporates it into a finite element model (FEM) with the crack path and geometry previously defined. This model has also been used for fracture prediction of adhesively bonded polymeric joints [31–34]. The CZM requires the definition of the traction separation law (T-s law) or CZM law of the crack (Fig. 2), where the stress in the crack interface and crack separation are related. In general, a CZM law consists of two parts:

1) Hardening: A linear relationship between the stress and separation until a maximum stress level is obtained. The adhesive and substrates suffer no damage or plastic deformations during this stage.
2) Softening: An increase in damage and decrease in stiffness as damage grows. Once the maximum stress is reached, damage begins. As it grows, stiffness is lowered. Unloading and reloading occur along a curve with lower stiffness, as seen in Fig. 2. The softening portion is not necessarily linear and is highly dependent on the adhesives, substrates, surface treatment, etc. The softening portion ends when damage reaches 1 (100%), which marks the total separation of the substrates.

The advantage of using a CZM is that it consists of a constitutive relation of the fracture that lumps all effects into one single non-linear relationship. However, this means that the CZM law must be obtained by experiments for a specific application. Preparing test specimens for these cases may not always be feasible since the test specimens may be large, and many may be required for repeatability and to define the test parameters and the shape of the CZM law. For fracture mode I parameters, a standardized test already exists (double cantilever beam test) [35] and is widely used [36–38]; however, there are still several proposals for improving the data processing, especially for reducing the

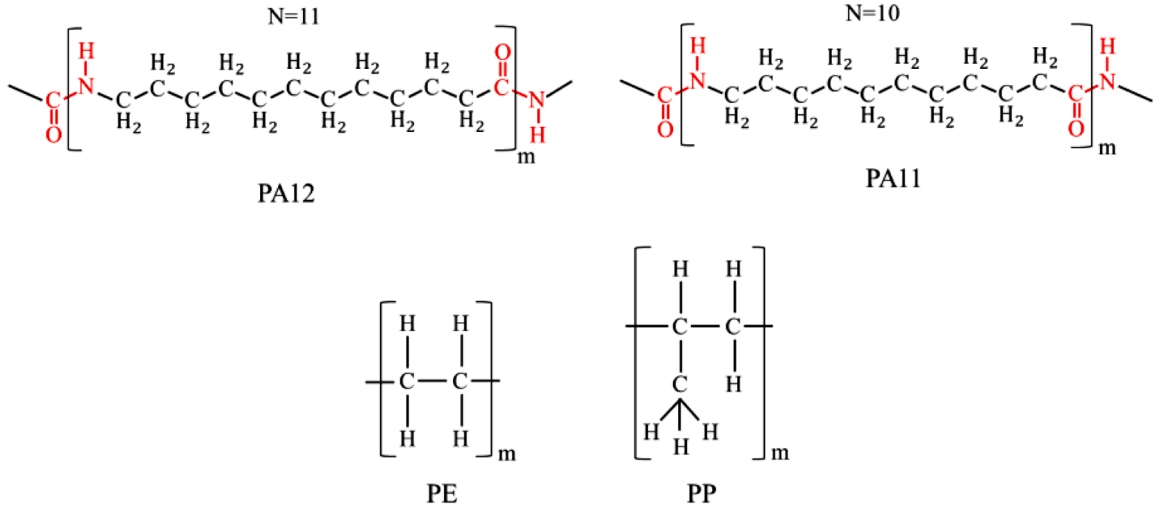


**Fig. 1.** Chemical structure of PA11, PA12, PP and PE (N: number of methylene groups between amide groups).

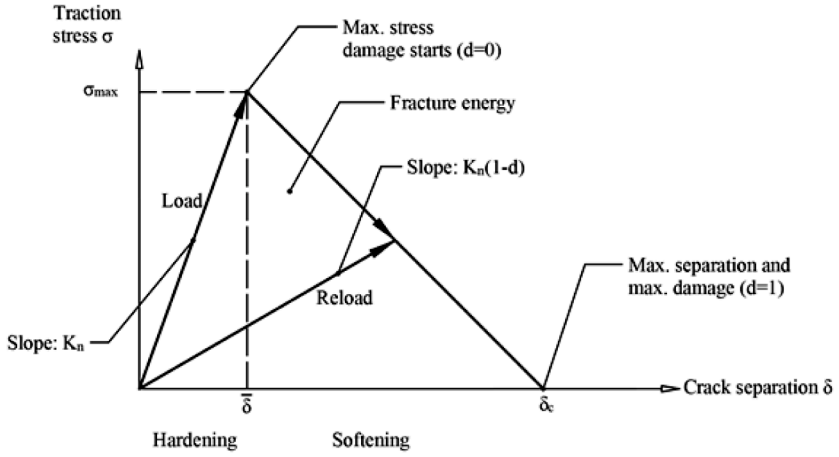


**Fig. 2.** Example of a bilinear CZM law and its stages.

need for crack length measurements [39,40]. Thus, employing a pull-off test to obtain the CZM laws for different adhesives with different surface treatments would prove to be a valuable alternative.

Although the APPT treatment of polyamides has been investigated recently, to the best of the authors' knowledge, research dedicated to the modification and comparison of PA11 and PA12 with the APPT technique besides numerical simulation of it has not been reported elsewhere.

## 2. Material and methods

### 2.1. Materials

Commercial polyamides (PA11 and PA12) were provided by Arkema (Madrid, Spain). Selected characteristic properties of the PAs are listed in Table 1 [41]. In order to evaluate the adhesion properties of PAs, rectangular plate specimens with dimensions of 80 mm × 180 mm × 4 mm were prepared by a hot plate press machine (Fontune Presses TPB374, Barendrecht, Netherlands). PA pellets were placed between the hot press plates with a specific program with a maximum temperature and pressure of 200 °C and 45 kN. According to the hot-press cycle, which is shown in Fig. 3, the gradual pressure steps were applied at 20 and 30 kN to facilitate densification and prevent air trapping. Moreover, each pressure step was held isothermally for 3 min.

Four commercial adhesives were used to perform the adhesion test: 2-component epoxy (Ceys, Araldite® Rapido, Barcelona, Spain), cyanoacrylate (Loctite®- Super Glue-3Precisión, HENKEL IBÉRICA SA, Barcelona, Spain), polyurethane (Sikaflex®−252 PU; Sika S.A.U. Madrid, Spain), and hybrid polyurethane (Sikaflex® −552 AT; Silane Terminated PU, Sika S.A.U. Madrid, Spain). Sikaflex®−252 and Sikaflex® 552AT are conventional single-component and hybrid single-component PU adhesive, respectively. The hybrid type is constituted by silane terminated PU, which assists in bonding on surfaces without primer or more complex surface treatments. The adhesives were applied in the laboratory with a controlled temperature of 22 °C and relative humidity between 27 and 30%.

Most epoxy resins are derivates from the reaction between A-bisphenol and epichlorohydrin. The addition of these two products creates linear chains with hydroxyl and epoxy groups, allowing further crosslinking through amines compost [42]. Araldite® cures in 10 min rapidly, but its maximum strength is achieved after 16 h when the ratio of hardener to resin is 1:1. It has a rigid behavior; thus, the adhesive thickness is 0.1 mm. When used to join polymers, it has a lower strength and needs surface treatment, as minimum abrasion and cleaning.

Polyurethane Sikaflex®−252 is a structural adhesive. It cures by atmospheric humidity, as diisocyanates and polyols compost all polyurethanes. Its behavior is elastomeric; thus, the adhesive thickness should be around 2 mm. Curing time depends on humidity and adhesive thickness, but as a minimum, it needs six days [43]. In addition, it joins metals and ceramics well, but tests should be done before joining polymers.

Cyanoacrylate is composed of ethyl cyanoacrylate. It is a rigid adhesive. It cures due to the humidity of the substrates in a matter of minutes but reaches maximum resistance after 12 h. Therefore, the thickness of adhesive between substrates is minimal (around 0.1 mm). It can join metals, ceramics, cardboard, wood and some plastics. However, it cannot bond with polyethylene, polypropylene, silicone, PVC, and glass [44].

**Table 1**
Characteristic properties of PAs.

| Property | PA 11 | PA 12 |
|---|---|---|
| Density (g/cm$^3$) | 1.03 | 1.01 |
| Yield stress (MPa) | 20 | 64 |
| Elasticity modulus (GPa) | 1.7 | 2.9 |
| Melting temperature ( °C) | 188–193 | 178–179 |

### 2.2. Plasma treatment

The Atmospheric Pressure Plasma Torch (Plasma treat GmbH, Steinhagen, Germany) was used to modify the polymers' surfaces (Fig. 4). The device setup and technical details were explained in the previous paper [25]. Air flux was fed to the system as a feeding gas. Three substrate-to-torch distances of 10, 20 and 30 mm were tested based on the water contact angle measurement. Also, the platform speed was set at two different values of 10 and 20 mm/s.

### 2.3. Polyamides wettability and surface energy

In order to evaluate the effect of plasma treatment on the PAs, their wettability was measured using three liquids with different polarities (deionized water, diiodomethane, and glycerol) before and after APPT treatment. The surface tension parameters of the mentioned liquids were obtained from the literature and are presented in Table 2 [45,46]. The static contact angle measurement according to the UNE-EN828:2013 standard was done with the sessile-drop method. In this regard, four drops of each liquid with a volume of 6 μl were deposited onto the polymer surface. The contact angle was measured after stabilization of the drop by Dataphysics OCA15 plus goniometer and SCA20 software (DataPhysics Instruments GmbH, Filderstandt, Germany). Then, the surface energy (SE) was calculated using the Owens-Wendt-Rable-Kaelble (OWRK) method [47], which considers

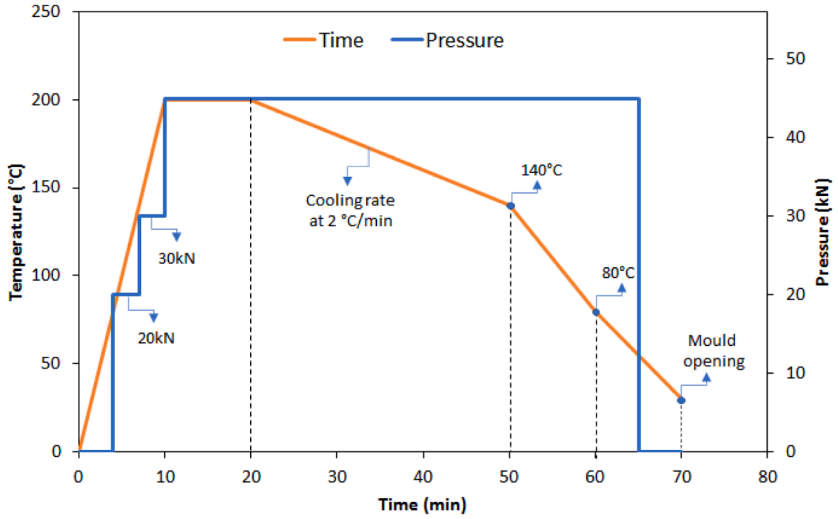


**Fig. 3.** Temperature and pressure profile during PAs hot-press.

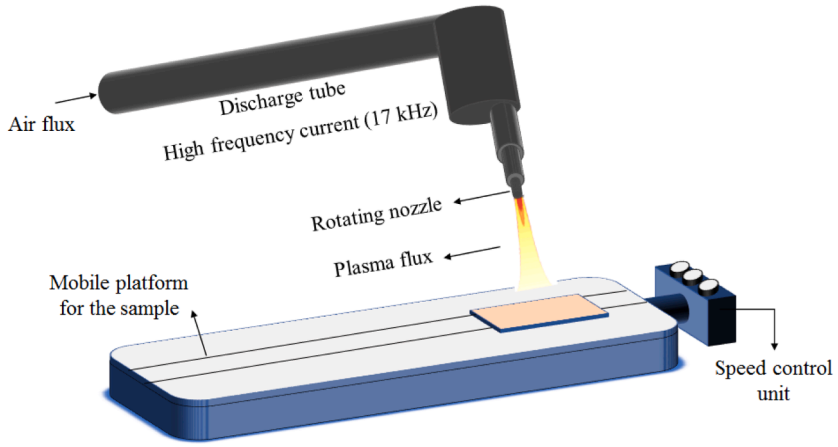


**Fig. 4.** Schematic of the APPT device.

**Table 2**
Polar and dispersive surface tension components of the test liquids at 25 °C for wettability measurement.

| Liquid | SE (mJ/m$^2$) | Disp (mJ/m$^2$) | Polar (mJ/m$^2$) |
|---|---|---|---|
| Deionized water | 72.8 | 21.8 | 51 |
| Diiodomethane | 50.8 | 50.4 | 0.4 |
| Glycerol | 63.4 | 34 | 30 |

various force components in the solid-liquid-vapor system formed during the drop deposition on the polymer surface.

The stability of material surface properties after the treatment is an essential parameter in the industry since the semi-product might be kept for a long time between the appropriate manufacturing steps. Thus, the effect of plasma treatment over time with different platform speeds of APPT device was also evaluated in this study. The contact angle test was done with different velocities (10 and 20 mm/s) after 10 min, 30 min, 11 days and 21 days of plasma treatment.

### 2.4. Chemical characterization of the surface by XPS and FTIR-ATR

The surface chemical composition of PA11 and PA12 was analyzed by X-ray photoelectron spectra (XPS) before and after plasma treatment by an ellipsoid scan probe with a major diameter of 400 μm which was calibrated based on the carbon peak (C—C/C—H, 284.6 eV). The XPS spectra were recorded on a Kratos XSAM 800 spectrometer (Kratos Analytical Ltd. Designs, Shimadzu Group Company, Manchester, UK), operating in fixed analyzer transmission mode, using Mg $K_\alpha$ (1253.6 eV) excitation. Survey spectra were recorded in the kinetic energy range of 0–1300 eV with 0.5 eV steps. Photoelectron lines of the principal constituent elements, like the $O_{1s}$, $N_{1s}$ and $C_{1s}$, were recorded by 0.1 eV steps.

The FTIR spectra of the PA plates before and after plasma treatment were recorded by an infrared spectrometer machine (Bruker Optik GmbH, Ettingen, Germany) equipped with an attenuated total reflection (ATR) technique to analyze the surface chemical modifications. The produced spectra were collected with a Bruker Tensor 27 spectrometer at the resolution of 4 cm$^{-1}$, 32 scans and an incident radiation angle of 45°. Three spectra were captured for each PA to ensure homogenous results.

### 2.5. Thermal characterization

Differential scanning calorimetry (DSC) analysis (DSC 822e, Mettler Toledo GmbH, Greifensee, Switzerland) was used to study the effects of APPT on the thermal properties of PAs surface. The DSC was performed with a heating rate of 20 °C/min in a temperature range of −60 °C to 200 °C. Moreover, the nitrogen as a purge gas was fed at a 50 ml/min rate.

### 2.6. Adhesion pull-off test

To study the effect of plasma treatment on the bond strength, the pull-off test was carried out based on the ISO 4624:2016 standard (ASTM Standard D 4541), using a Universal Testing Machine EM1/200FR (Microtest, Madrid, Spain) at a rate of 0.5 mm/min at room temperature with a load cell of 1 kN, using aluminum dollies of 20 mm diameter (Fig. 5a). The test determines the highest perpendicular force (in tension) that a polymer can bear as a substrate before an adhesive plug is detached. After the adhesion tests, the mechanism of the adhesives' detachment was also evaluated.

The polymer surfaces for adhesion tests were first polished with silicon carbide abrasive paper (grit number P1200 and 2000) and then cleaned with acetone. Then the APPT was employed on half of the samples' surfaces (Fig. 5b). The adhesives were applied onto the polymer surface with a controlled thickness of 2 mm (for PU and PU-hybrid adhesives) and 0.1 mm (for the epoxy and CA adhesives). The thicknesses for PU and PU-hybrid were controlled by small glass balls with an appropriate diameter and for epoxy and CA with a weight of dolly through the proper support. Six dollies were used for each adhesive to perform the pull-off test. According to the manufacturer's recommendation, prior to using the PU adhesive, Sika® Primer-210 was applied on the aluminum dolly surface to react with moisture and form a thin layer, which links polymer and adhesives.

### 2.7. Surface morphology

In order to evaluate the effect of the APPT treatment on the surface morphology, roughness analysis of the treated and untreated specimens was carried out by Motorized Microscope System (BX61, Olympus Corporation, Tokyo, Japan), which provides 3D surface images. The surfaces were scanned with 280X magnification. Moreover, the mean areal surface roughness ($S_a$) was calculated for each polymer according to Eq. (1)

$$S_a = \frac{1}{MN}\sum_{j=1}^{N}\sum_{i=1}^{M} z(x_i; y_j)\Bigg) \quad (1)$$

where z is the height of the measured points in the coordinates of x and y [48]. This equation measures surface roughness based on the average absolute vertical deviation of all data points. Furthermore, other roughness parameters such as $S_{pk}$, $S_k$, $S_{vk}$, $S_{Mr1}$, and $S_{Mr2}$ can be derived from the Abbott-Firestone curve [49], which is presented in Fig. 6 [50].

$S_{pk}$, the reduced peak height, represents the peak height above the core roughness. $S_k$, the core roughness depth, shows the peak-to-valley (core roughness) distance of the surface with the predominant peaks and valleys. $S_{vk}$, the reduced valley depth, is the valley depth below the core roughness. $S_{Mr1}$ and $S_{Mr2}$ indicate the percentage of material that comprises the peak and valley structures associated with $S_{pk}$ and $S_{vk}$, respectively.

### 2.8. Adhesion pull-off test simulations

The numerical simulations were carried out in ANSYS 2021 as a static analysis due to the low velocity of the tests. The numerical model consists of an aluminum cylinder, representing the dolly, where a displacement was applied on the upper face; a polymer cylinder representing the substrate, which was fixed to the ground; and a layer of contact elements with CZM (cohesive zone modeling) capabilities in between, which were representative of the adhesive and its surface treatment altogether. These contact elements have zero thickness. The dolly and the substrate were modeled as linear elastic materials, while the adhesive was considered as bilinear CZM contact elements. The model is depicted in Fig. 7. The parameters for the CZM properties are based on the experimental pull-out test results as follows:

- The initial linear portion of the force-displacement curve is taken as the contact stiffness of the CZM elements.
- The maximum force is used to determine the maximum stress in the CZM model.
- The maximum displacement measured during the test is used as the maximum separation.

These parameters are used for a bilinear CZM law, similar to the one depicted in Fig. 2.

## 3. Results and discussion

### 3.1. Polyamides wettability and surface energy

Tables 3 and 4 show the surface energies, including both polar and dispersion components. They are presented for 10 mm/s and 20 mm/s as a platform speed for treatment optimization. Based on the reported values, both velocities led to the similar surface energy after 10 min. However, with the lower velocity of 10 mm/s, the energetic ionized gas of plasma had more time to alter the physicochemical nature of polyamides' surfaces, which resulted in higher durability of plasma on the surface over the time. This behavior is more tangible after 30 min of APPT treatment. The surface energy of polyamides significantly decreased after 30 min for the higher velocity of 20 mm/s, while 10 mm/s could keep the same range of energy after 30 min. Therefore, the 10 mm/s was used in further comparative experiments. Moreover, the substrate-to-torch distance was set to 10 mm since it had a lower water contact angle with respect to 20 and 30 mm; in addition, less than 10 mm, plasma degraded the substrate surface.

In Table 5, the contact angle values of water, diiodomethane and glycerol are listed. The surface energy values were calculated, including both the polar and dispersive components for the untreated and plasma-treated samples and shown in Fig. 8. The untreated polymers were found to be rather hydrophobic, with their high-water contact angle values being 93° and 83° for PA11 and PA12, respectively. APPT treatment could greatly decrease the contact angles, which sums up to at least a 22% reduction for each reference liquid. The high decrease in the water contact angle indicates a high increase in the polarity of the surfaces after the treatment because the water molecule is polar. Moreover, the total surface energy significantly increased, mainly due to the rise of polar components. Compared with untreated PA11 and PA12, there was an approximate increase of 40% and 85% in surface energy, respectively. The polar component also follows the same trend observed with surface free energy. The reduction of wetting contact angles tightly

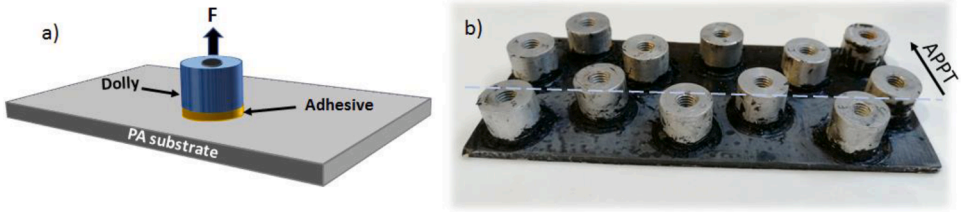


**Fig. 5.** a) Schematic of a pull-off test, b) test configuration for each polymer substrate.

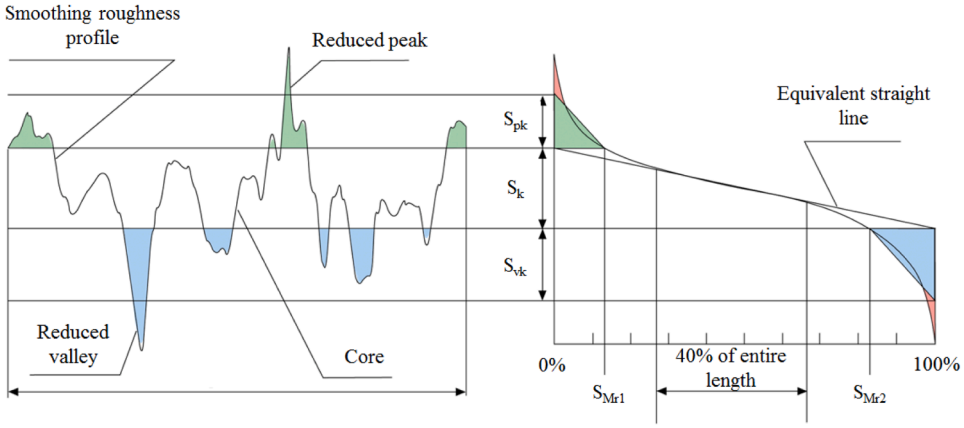


**Fig. 6.** Abbott-Firestone curve showing the construction of the $S_k$ family parameters.

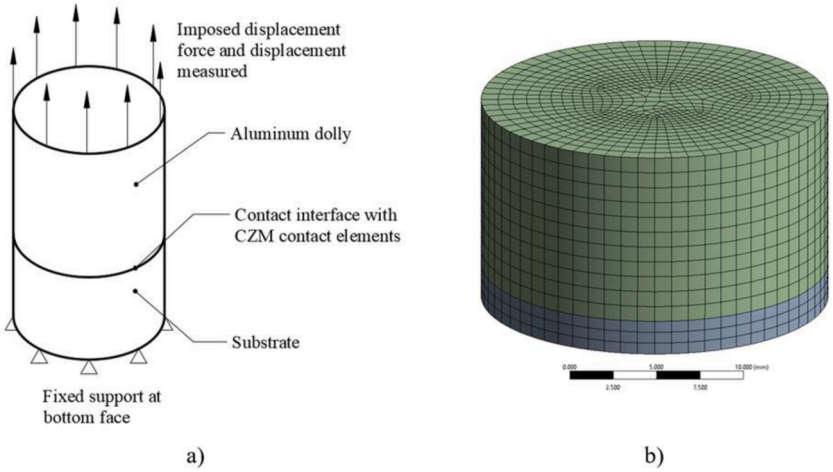


**Fig. 7.** a) Scheme of the numerical model, b) mesh used for the simulations.

**Table 3**
Effect of plasma velocity on the surface energy of PA11 and PA12: 10 mm/s velocity.

| 10 mm/s | 10 min after treatment | | | 30 min after treatment | | |
|---|---|---|---|---|---|---|
| | SE (mJ/m$^2$) | Disp (mJ/m$^2$) | Polar (mJ/m$^2$) | SE (mJ/m$^2$) | Disp (mJ/m$^2$) | Polar (mJ/m$^2$) |
| PA11 | 58.37 | 9.20 | 49.17 | 60.18 | 19.46 | 40.72 |
| PA12 | 58.5 | 9.36 | 49.14 | 61.64 | 22.32 | 39.32 |

**Table 4**
Effect of plasma velocity on the surface energy of PA11 and PA12: 20 mm/s velocity.

| 20 mm/s | 10 min after treatment | | | 30 min after treatment | | |
|---|---|---|---|---|---|---|
| | SE (mJ/m$^2$) | Disp (mJ/m$^2$) | Polar (mJ/m$^2$) | SE (mJ/m$^2$) | Disp (mJ/m$^2$) | Polar (mJ/m$^2$) |
| PA11 | 58.31 | 16.44 | 41.87 | 35.84 | 25.82 | 10.03 |
| PA12 | 58.5 | 9.36 | 49.14 | 33.35 | 20.52 | 12.84 |

corresponds with these surface energy changes. Based on the wetting theory [51], in order to have a high-performance adhesive bond, the surface energy of adherend should be higher than applied adhesive.

Fig. 9 shows the evolution of the treatment over time, where time zero corresponds to the untreated sample. Before treatment, the surface

**Table 5**
Contact angle values of the treated and untreated PAs.

| Polymer | $\theta_W$ (°) | $\theta_{CH2I2}$ (°) | $\theta_{GI}$ (°) |
|---|---|---|---|
| PA11 | 93±2 | 62±1 | 97±1 |
| PA12 | 83±5 | 63±1 | 82±2 |
| PA11-APPT | 26±3 | 48±6 | 41±4 |
| PA12-APPT | 22±4 | 40±6 | 61±6 |

energy was higher for PA11 than PA12 (42 vs. 32 mJ/m$^2$); however, untreated PA12 had a higher polar component than PA11 (6 vs. 2 mJ/m$^2$). Once the surface treatment had been carried out, the surface energies for the two polyamides were equalized to around 58 mJ/m$^2$after 10 min. This increment in the total surface energy corresponds fundamentally to the polar component increment, while the dispersive component decreased when the samples were tested after APPT. Contrary to what was previously reported for other polymers [26] that surface hydrophobicity recovered after approximately 30 min of storage, the effect of plasma treatment has not vanished even after 11 days for PAs. Over time, the total surface energy increased slightly and the dispersive tended to that of the untreated sample. Thus, on the 11th day, the total surface energy was 35% and 51% higher than the initial for PA11 and PA12, respectively. However, the polar component has decreased by 1% for PA11 and 4% for PA12 on the 11th day. The aging of the treatment continues until 21 days, to which the polar component has reduced by 10% for PA11 and 34% for PA12, higher than initial values but not sufficient for good wettability. This reduction in surface

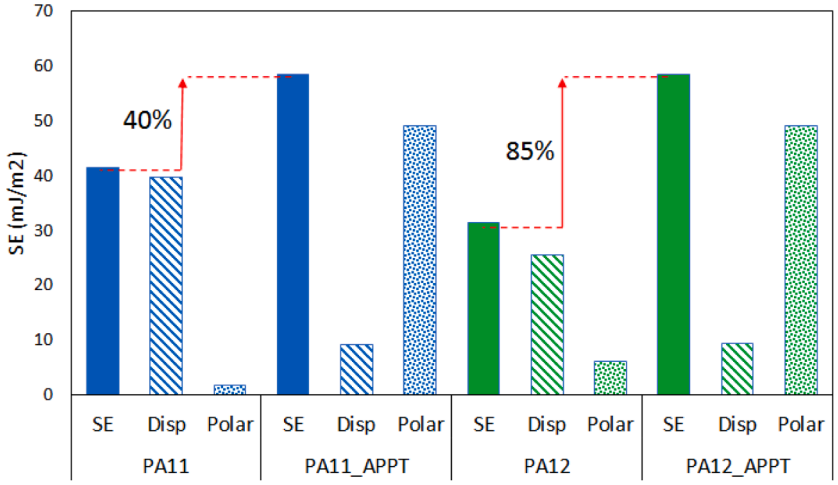


**Fig. 8.** Comparison of surface energy components before and after APPT treatment of PA11 (blue) and PA12 (green). (For interpretation of the references to colour in this figure legend, the reader is referred to the web version of this article.)

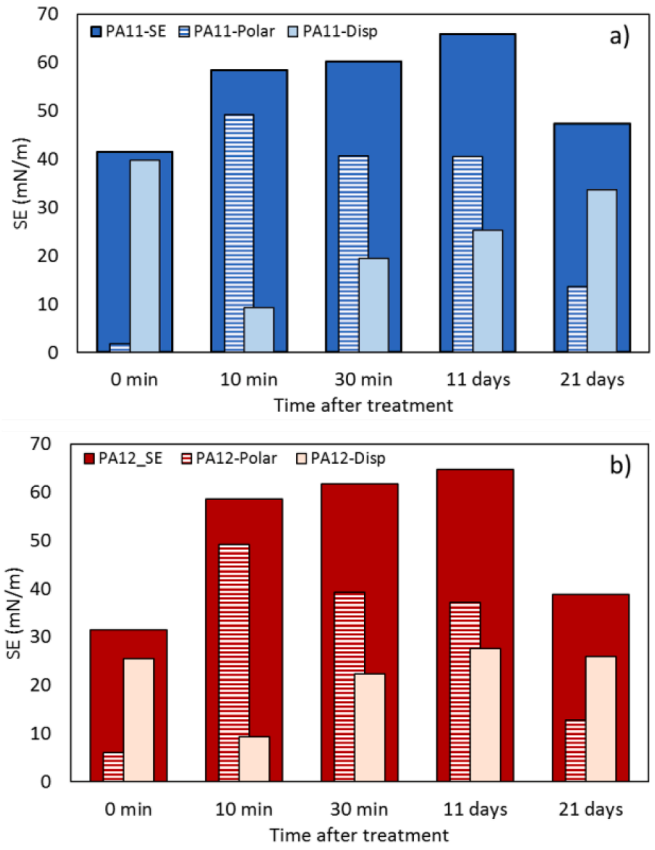


**Fig. 9.** Comparison of surface energies after different times from APPT treatment: a) PA11, b) PA12.

energy and wettability after 21 days is due to the surface reactivity and thermodynamically driven reorientation of polar groups away from the surface into the bulk [52].

Accordingly, from an application point of view, the achieved results propose that for applying coatings, adhesives or any other functionalizing processes on the plasma-activated polyamides, they can be expanded in time (around 11 days) after plasma treatment; in this way, the polar component of the surface energy has a considerably higher value than untreated surfaces.

### 3.2. Chemical characterization of the surface

#### 3.2.1. XPS analyses

The elemental compositions (atomic%) of the polyamides surfaces before and after plasma treatment calculated from the survey spectra are presented in Table 6. The survey spectrum of hot-pressed PAs in Fig. 10 shows the presence of carbon, oxygen, and nitrogen, as predicted from the chemical structure ($C_{11}H_{21}NO$ and $C_{12}H_{23}NO$). Furthermore, the utilized polyamides include some additives or fillers such as P, Ca and Na, which are beneficial for optimizing the polymer properties [53,54]. After APPT treatment, the concentration of the individual chemical elements changed. Compared to the untreated polyamides, the amount of oxygen and nitrogen increases while the amount of carbon decreases. Moreover, Table 6 illustrates how APPT treatment increases the O/C and N/C ratios. Furthermore, the energetic ionized gas of the plasma source has affected some of the PA11′ fillers, which resulted in the formation of $P_2O_5$ (134.08 eV (P2s) and 191.8 eV (P2p)), NaCl (1072 eV), $CaCO_3$ (348 and 351 eV). These polar and ionic groups are able to form strong chemical/physical interactions with the adhesives and improve adhesion bonding with the absorption mechanism [47]. This change in filler compounds is more evident in PA11 since using plasma, fillers migrate from inside the PA11 to the surface, in contrast to PA12, in which fillers are inside and on the surface before plasma treatment..

The peak fitting routines were done to evaluate the bond structure changes. Fig. 11 and 12 show the deconvolution results for the $C_{1s}$, $N_{1s}$ and $O_{1s}$ XPS spectra of PAs surfaces before and after the plasma. The $C_{1s}$ spectrum was fitted with four peaks, which are identified as aliphatic carbon atoms (C–C/C–H, 284.58 eV), carbon atoms bonded to the -NH groups (C–N, 285.59 eV), single-bonded carbon to oxygen (C–O, 286.57 eV) and carbon atoms of carbonyl groups (C = O, 288.27 eV). The presence of C—O bond on the untreated surfaces can be assigned to the contamination of the surfaces or partial atmospheric oxidation of the main chain of the PAs (during the hot press process). Since the hot press chamber was not vacuumed, the high temperature of the process (200

**Table 6**
The Surface composition (atomic%) of the treated and untreated PAs determined by XPS.

| | PA12 | PA12-APPT | PA11 | PA11-APPT |
|---|---|---|---|---|
| C% | 62.24 | 42.36 | 70.16 | 42.05 |
| O% | 24.89 | 38.9 | 16.87 | 42.81 |
| N% | 12.86 | 16.56 | 12.96 | 13.05 |
| O/C% | 39.99 | 91.83 | 24.05 | 101.81 |
| N/C% | 20.66 | 39.09 | 18.47 | 31.03 |

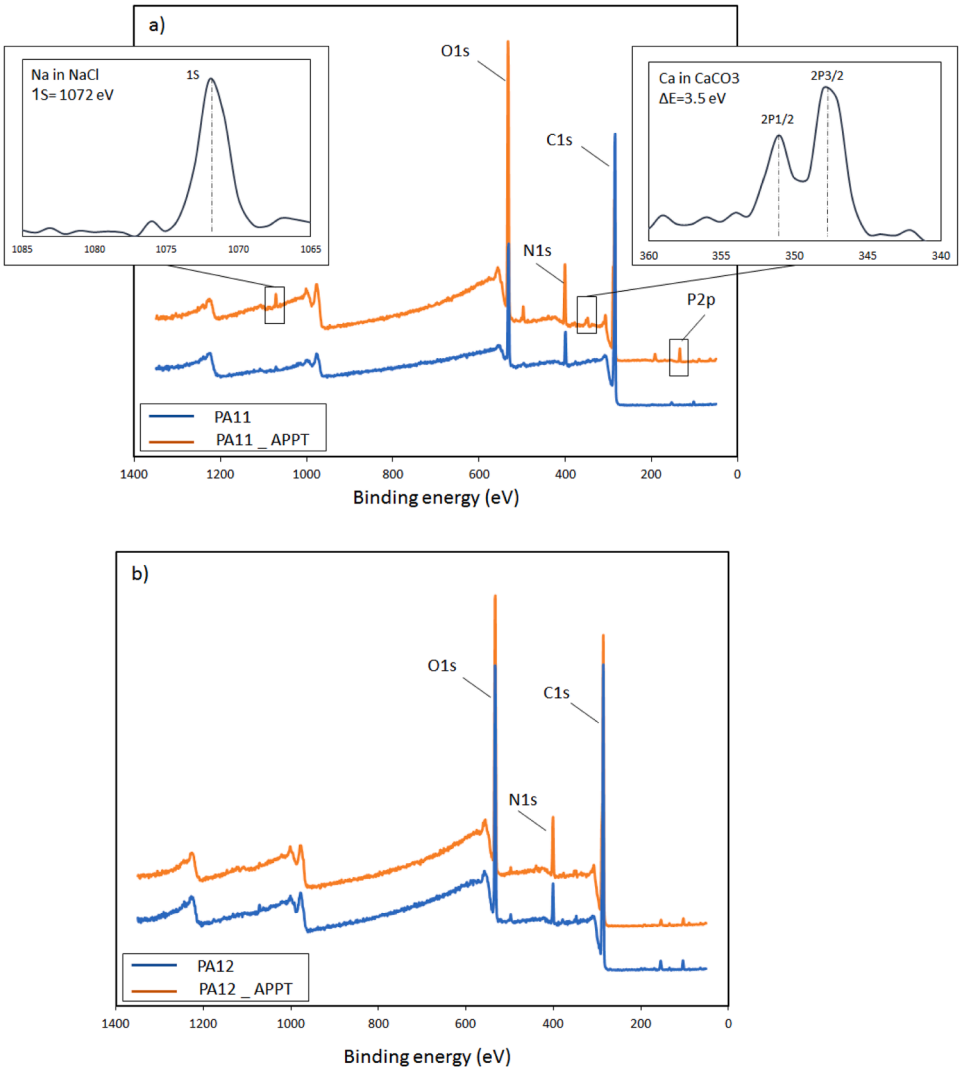


**Fig. 10.** XPS spectra of treated and untreated polyamides; a) PA11, b) PA12.

°C) may facilitate the atmospheric oxidation of PA pellets during the press; polyamides are such types of thermoplastic polymers that can be readily oxidized when heated above their melting temperature [55]. After APPT treatment, the intensity area under the peaks corresponding to the C–C/C–H and C–N decreased by 19% and 14% respectively for PA11 (Fig. 11a) and by 15% and 19% for PA12 (Fig. 12a), whereas the intensity of C–O and C = O peaks respectively increased by 8% and 25% for PA11 and by 11% and 22% for the PA12. By classifying the functional groups into polar and nonpolar, we can quantify the changes in the surface composition by comparing the polar to nonpolar intensity ratio. Peak C–C/C–H is a nonpolar group and the rest are polar. This ratio increased from 0.61 to 1.32 for PA11 and from 0.73 to 1.33 for PA12. This is the main reason for increasing the wettability. An increase in carbon-oxygen bonds concentration would be due to the recombination of reactive sites formed on the surface of the polyamides with free oxygen radicals in the plasma.

These changes are also evident in the deconvolution of $O_{1s}$ spectra (Fig. 11b and12b). The peaks correspond to the polar groups, including oxygen bonded with carbon and carbonyl. The intensity of all these three peaks increased after the plasma treatment. In addition, the analysis of the $N_{1s}$ spectrum showed that plasma had excited the antibonding sigma bonds of orbital 1 s (Fig. 11c and12c). Antibonding sigma level has more energy than bonding sigma and $1_S$ orbital; thus, plasma provided more active sites for reaction with adhesives.

### 3.2.2. FTIR-ATR analyses

The FTIR spectra of treated and untreated PAs are illustrated in Fig. 13. Both PA11 and PA12 have very similar peaks. The absorption peaks at 1635 $cm^{-1}$, 1540 $cm^{-1}$ and 1275 $cm^{-1}$, which are assigned to amide I, amide II and amide III, respectively, are the most typical peaks of PA11 and PA12 [56]. The intense bands at 2850.7 $cm^{-1}$ and 2918.2 $cm^{-1}$ belong to symmetric and antisymmetric stretching vibrations of the C—H group, respectively [56]. The complete curve-fitting results for PA11 and PA12 were listed in previous work [41]. After APPT treatment, the peak intensity of amid I and II increased by 19% and 18% respectively for PA11 and by 8% and 16% for PA12, meaning the presence of more functional groups of C = O and $NH_2$, which agrees with the XPS results. It is worth mentioning that these increases are lower than XPS because the infrared scan depth is more remarkable than XPS.

## 3.3. Thermal characterization

Thermal properties including melting temperature ($T_m$), melting enthalpy (ΔH) and degree of crystallinity ($X_c$) were measured by DSC for PA11 and PA12 before and after treatment and are summarized in Table 7. Moreover, the typical heating thermographs for each PA are compared in Fig. 14. The presented results are consistent with a previous paper by the authors [41] and show that the plasma treatment did not significantly affect the thermal properties of the PAs. This means the

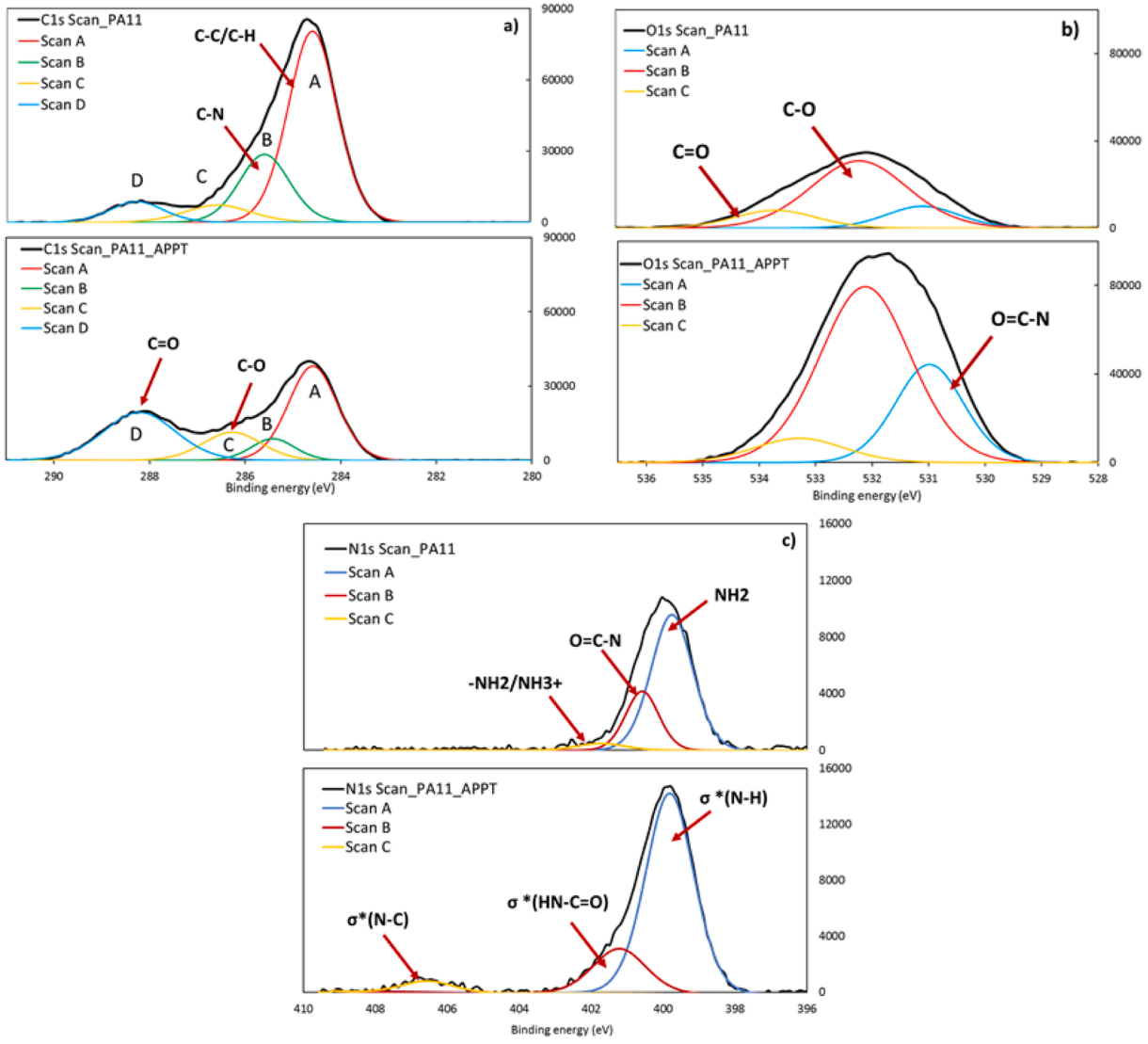


**Fig. 11.** XPS spectra as a function of binding energies of the untreated (up) and plasma-treated PA11(down): a) $C_{1s}$, b) $O_{1s}$, c) $N_{1s}$.

thermal stability of PAs did not compromise with APPT treatment which is essential for any surface treatment technique. The minor differences found in Table 7 are within the measurement error.

### 3.4. Adhesion pull-off test

Fig. 15 displays the adhesion strength of different adhesives with PA11 and PA12. Epoxy and PU-hybrid had the highest adhesive strength among the other adhesives applied on the PAs. The most considerable growth of adhesive strength after APPT treatment was found for the epoxy. In this case, the adhesive strength increased from 0.86 MPa to 2.2 MPa for PA11 and from 0.67 MPa to 2.6 MPa for PA12, translating to approximately 157% and 291% growth, respectively. The positive effect of plasma treatment on epoxy bonding strength can be attributed to the reaction of epoxy groups with functional groups produced after plasma exposure that create covalent linkages between adhesive and polymer surface.

The analysis of variance (ANOVA) was applied to the adhesion strength values of treated and untreated polymers for each adhesive to evaluate the distribution of results. In ANOVA, there are two main parameters of F and $F_{critical}$. Suppose the calculated value of F critical is more than the standard tabulated value of the F for a given confidence interval. In that case, there is no significant difference between the results, and they are similar within the confidence limit. The average of adhesive strengths for each adhesive besides the ANOVA outcomes at 95% confidence interval (alpha = 0.05) are presented in Table 8. According to this table, the $F_{critical}$ is only lower than the F value for epoxy adhesive, meaning that the APPT treatment had not significantly affected CA, PU, and PU-hybrid adhesives' adhesion strength.

Regarding the PU-hybrid, although the average value of strength was increased after APPT, this modification is not significant based on ANOVA. This effect is rational since silane added to PU improves the adhesion by chemical anchor between adhesive-substrate. Given the CA, the curing mechanism is a moisture-based process that requires humidity on the substrate surface. However, the plasma treatment completely dries the surface, which prevents adhesion improvement. Regarding PU, no improvement in adhesive strength might be due to the low polar surface tension of PU (5.4 $mJ/m^2$ [57]). The surface tension of adhesives must be lower than the surface energy of solid substrates for the proper bonding; however, this difference should not be too high. PA has high dispersive surface energy and low polar component. Therefore, they can be joined to dispersive adhesives such as polyurethane but with low strength without treatment since they have similar polar component energy. However, after APPT, the polar component energy of PA increased a lot, resulting in too much energy difference between PA and PU.

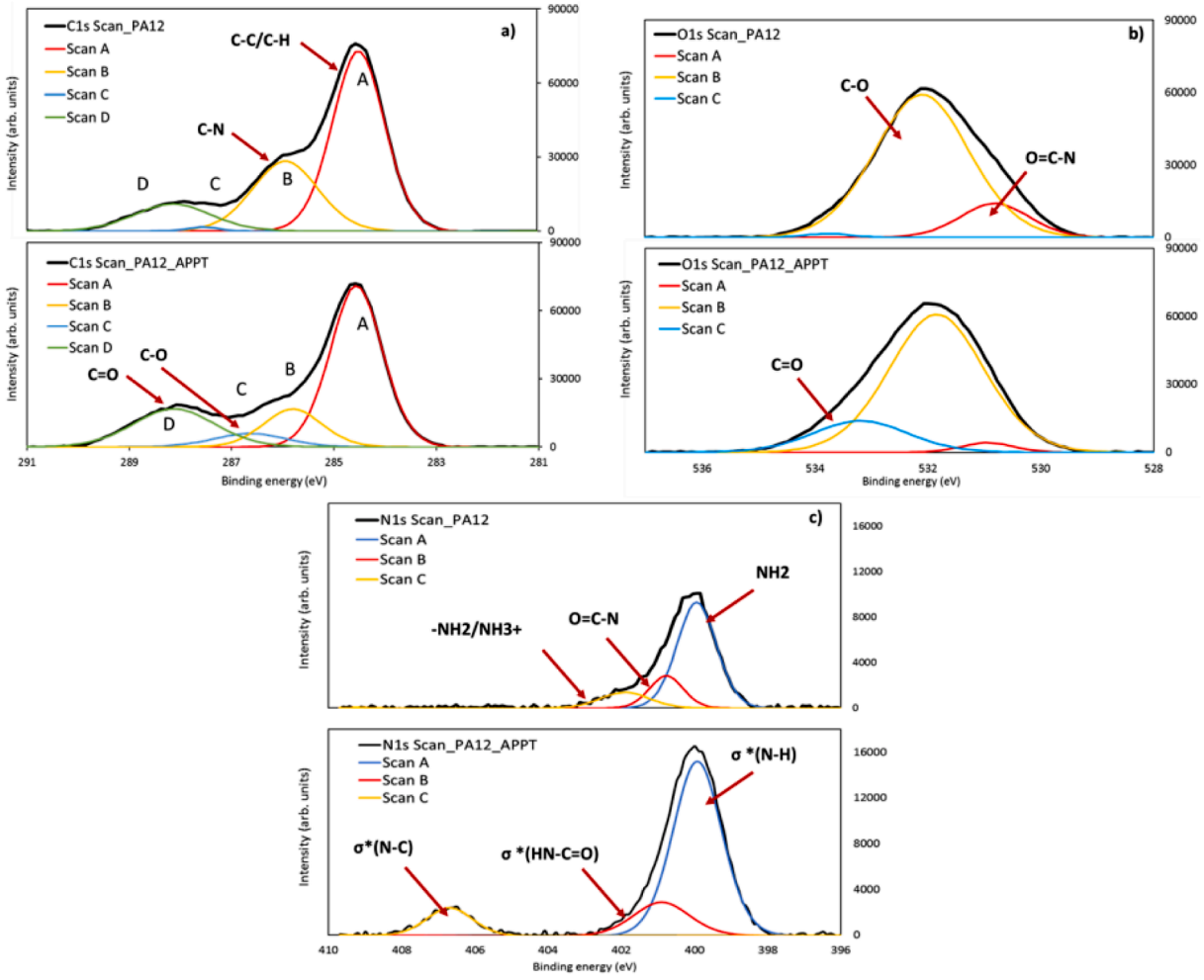


**Fig. 12.** XPS spectra as a function of binding energies of the untreated (up) and plasma-treated PA12 (down): a) $C_{1s}$, b) $O_{1s}$, c) $N_{1s}$.

On the other hand, the adhesion strengths of Table 8 give the impression that the APPT treatment did not affect the bonding strength of the adhesives except epoxy. However, evaluation of the adhesive failure is an essential part of the adhesion test. Five failure modes are possible depending on the location of the failure interface, Mode A through E, as shown in Fig. 16 [58]. The first mode (A) indicates adhesive pulled off from the dolly surface. Mode B shows adhesive failed with partially cohesive-adhesive failure. In mode C, the adhesive detached from the surface of the substrate. Mode D is similar to mode C, in which part of the substrate is also detached. The last mode (E) is a cohesive failure in the PA substrate. According to Fig. 17, before plasma treatment, epoxy, CA and PU-hybrid failed with mode C and the PU-hybrid adhesive failed with mode B.

After APPT treatment, the epoxy adhesive had approximately similar failure modes for both PAs. Although in the case of epoxy/PA11, tiny parts of the substrate detached by adhesive (mode D), there were also a few cases for epoxy/PA12 with mode D (not the majority). TheCA and PU-hybrid failure modes changed to B and A, respectively. Both last detachments indicate a stronger interface bond between adhesive to the surface of polyamide substrate compared to untreated samples. In this regard, the reported adhesive strengths for PU-hybrid and CA after APPT are not the exact forces required for adhesive pull-off from PA; instead, they are the breaking forces of adhesives exclusively. Thus, it can be concluded that the adhesion strength of CA and PU-hybrid adhesives after APPT treatment increased. On the other hand, the unchanged failure mode of PU specifies no effect of APPT.

### 3.5. Surface morphology

The 3D images captured by BX61 microscopy from polymers surfaces are shown in Fig. 18. The roughness parameters which were calculated based on the Abbott-Firestone curve and Eq.1, are also presented in Table 9. It is seen that APPT treatment reduced the $S_a$ parameter of surfaces by 34% and 28% for PA11 and PA12, respectively. The 3D images also exhibit the smoother surface of treated surfaces, which could be due to the cleaning and ablation effect of plasma which also has been reported previously [59–62]. Surface ablation is very common in plasma treatment processes which happens due to the hydrogen removal that causing weight loss in the treated surface [63,64].

Lower $S_{pk}$ and $S_{vk}$ of APPT treated polyamides imply that plasma has smoothed the peaks and filled the valleys of the surfaces. Lower $S_k$, which is the distance of peak-to-valley or core roughness, is another proof of roughness reduction after APPT. However, higher $S_{Mr1}$ indicates that plasma treatment increased the amount of materials with peak structures associated with $S_{pk}$. The reduction of micro-roughness causes lower mechanical interlocking of a substrate with other substances. In other words, lower roughness resulted in lower surface area for a chemical reaction, which might be another reason for the unchanged bonding strength of CA, PU and PU-hybrid adhesives.

### 3.6. Numerical simulation results

#### 3.6.1. CZM parameters obtained from pull-off tests

Following the procedure indicated in Section 2.8, the following

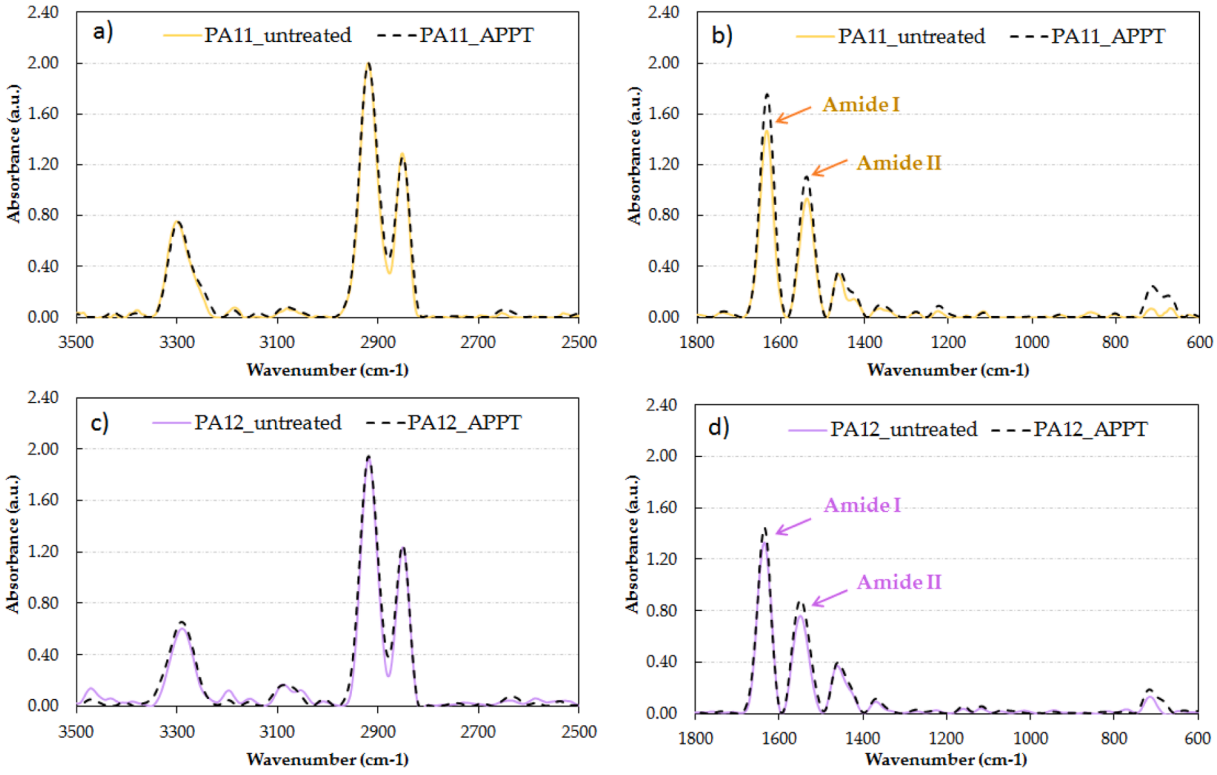


**Fig. 13.** FTIR spectra of hot-pressed PAs before and after treatment: a,b) PA11, c,d) PA12.

**Table 7**
Thermal properties of studied Pas by DSC measurements.

| | PA11 | | PA12 | |
|---|---|---|---|---|
| | Untreated | APPT | Untreated | APPT |
| $T_g \pm 2$ (°C) | 44 | 42 | 43 | 46 |
| $T_m \pm 3$ (°C) | 193 | 190 | 179 | 181 |
| $\Delta H \pm 2$ (J/g) | 52 | 50 | 47 | 45 |
| $\chi_c \pm 2$(%) | 23 | 22 | 49 | 47 |

parameters were extracted for a bilinear CZM law: the corrected strength, the contact stiffness for the simulations, and the maximum crack separation. These parameters can also be used to obtain the critical fracture energy (area under the CZM curve) and compare it with the experimental value. The summarized results are shown in Table 10.

It should be noted that there is a great dispersion of the data results, particularly in the maximum crack separation results. Thus, the averages are shown and used for the simulations.

### 3.6.2. CZM parameters obtained

Based on the experimental and numerical results, meaningful results could be obtained. It is noted that the substrate (whether PA11 or PA12) has little or no influence on the shape of the CZM law; however, the adhesive and the surface treatment do have a significant influence, as detailed below.

For the case of the epoxy adhesive, the bilinear CZM law worked adequately for both substrates, mainly due to the brittle nature of the epoxy, as shown in Fig. 19. Not only the adhesive strength increased with the APPT, but so did the fracture energy and, more importantly, the stiffness. The most significant increase was seen with the PA11, where the adhesive could partially hold the load after reaching the load peak. The results in Fig. 19 also show that the epoxy adhesives greatly benefit from the APPT treatment, as the peak load is significantly increased. Unlike other adhesives, the PA12 showed a significant reduction in the maximum displacement during the pull-off test. It is theorized that this

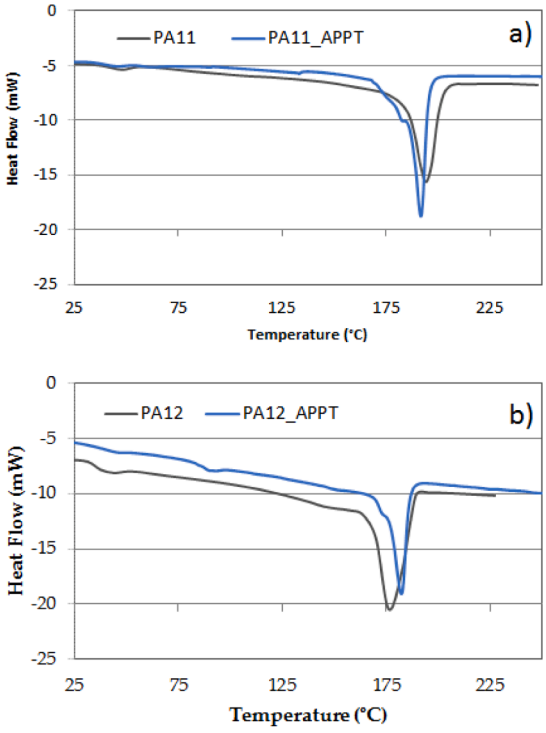


**Fig. 14.** DSC thermograms of PAs before and after treatment (heating rate: 20 °C /min): a) PA11, b) PA12.

difference comes from the higher surface roughness present in the untreated PA12, as shown in Table 9. It can also be deduced that the epoxy adhesives are far more sensitive to changes in the surface roughness than other adhesives, which do not show this change. This behavior is

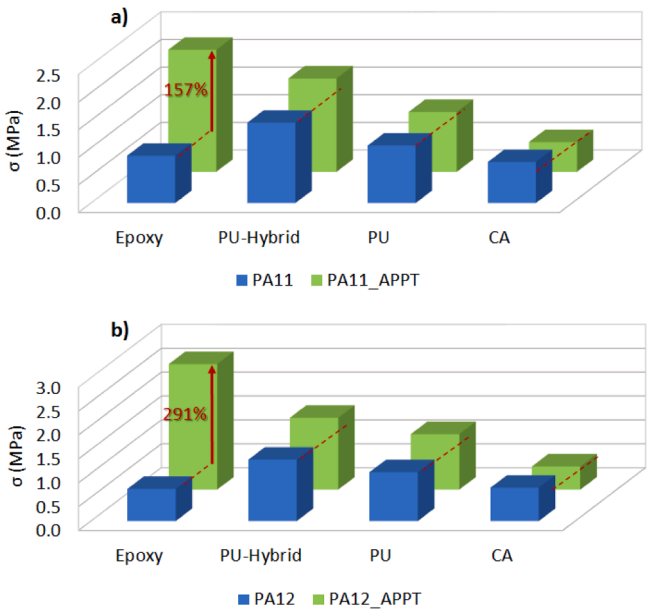


**Fig. 15.** Variation of adhesion strength of different adhesives for treated and untreated PAs: a) adhesion strength of PA11, b) adhesion strength of PA12.

**Table 8**
ANOVA results for adhesion strength of PA11 and PA12 with different adhesives.

| Adhesive | AVG adhesion strength (MPa) | Mean square | F | F critical |
|---|---|---|---|---|
| PA11 | | | | |
| Epoxy-APPT | 2.208 | 6.231 | 118.940 | 4.965 |
| Epoxy | 0.857 | | | |
| PU-hybrid-APPT | 1.691 | 0.167 | 2.869 | 4.965 |
| PU-hybrid | 1.455 | | | |
| PU-APPT | 1.084 | 0.006 | 0.595 | 4.965 |
| PU | 1.040 | | | |
| CA-APPT | 0.539 | 0.104 | 2.953 | 5.317 |
| CA | 0.744 | | | |
| PA12 | | | | |
| Epoxy-APPT | 2.628 | 11.479 | 305.154 | 4.965 |
| Epoxy | 0.672 | | | |
| PU-hybrid-APPT | 1.502 | 0.141 | 4.191 | 4.965 |
| PU-hybrid | 1.286 | | | |
| PU-APPT | 1.051 | 0.060 | 4.898 | 4.965 |
| PU | 0.909 | | | |
| CA-APPT | 0.577 | 0.043 | 0.442 | 4.965 |
| CA | 0.698 | | | |

consistent in all tests.

Similarly, the bilinear CZM law also fitted the CA adhesive appropriately due to its brittle nature, as shown in Fig. 20. The plasma treatment did provide a more significant maximum crack separation on average. There was an apparent loss in strength for the PA11 substrate with APPT, which might occur due to the large dispersion in the results (recall Table 8), and the average was used. This dispersion might also be responsible for the apparent disagreement in the maximum crack separation.

As for the PU adhesive, the bilinear law reproduced the results with some errors, as seen in Fig. 21. The main difference is that the experimental results have a non-linear hardening portion near the peak stress. A trapezoidal or trilinear CZM law could be used to overcome these issues for substrates with and without APPT. Although there was no significant increase in the adhesive strength, the fracture energy increased for the APPT treated PAs. It is also worth noting that the low contact stiffness affected the stability of the numerical simulation. To obtain the full test curve, a mesh element size lower than that of Fig. 7 was used, as well as very low load increments, represented as a low simulation time step. The red stars in Fig. 21 and Fig. 22 correspond to the points where the mesh size and time step were decreased to ensure numerical convergence; before these points, the original mesh was used for the modeling.

Finally, the PU-hybrid adhesive case showed the most significant change in the shape of the CZM-law (Fig. 22). In the case of untreated PAs, the bilinear CZM law reproduced the experimental results with acceptable accuracy. However, the specimens with APPT could hold the peak load, which means they were able to absorb more significant fracture energy. This, in turn, means that a trapezoidal CZM law could fit the data better. However, it must be noted that for both evaluated cases: to obtain the complete curve, a simulation with a much smaller mesh element size and much lower solution time step was required. The mesh shown in Fig. 7 could only reach the point marked in the red star in Fig. 22 before separation/termination. However, decreasing the element size and time step can significantly increase the simulation time.

The utilized bilinear CZM law proved to be adequate for simulating brittle adhesives with and without treatment. However, it is inadequate for the more elastic adhesives, which could be better described with a trapezoidal CZM-law. It is also worth noting that cases with low contact stiffness (elastic adhesives) require a very fine mesh with small time steps (or load increments) to reproduce the whole test curve.

## 4. Conclusions

Surface modification of polymers by atmospheric pressure plasma is a well-known technique typically performed before any bonding. This study has provided a methodology of surface improvement by employing APPT treatment on the PA11 and PA12 surfaces. In this regard, various surface characterization techniques were applied to verify the plasma effects on the surfaces. Based on the performed experiments and analyses, the conclusions were obtained as follows:

- The wettability of surfaces was improved significantly by reducing the contact angles and increasing surface free energy by 40% and 85% for PA11 and PA12, respectively.
- Plasma-activated polyamide surfaces did not lose their high polar surface energy until 11 days after treatment, showing their stable functionality over time.

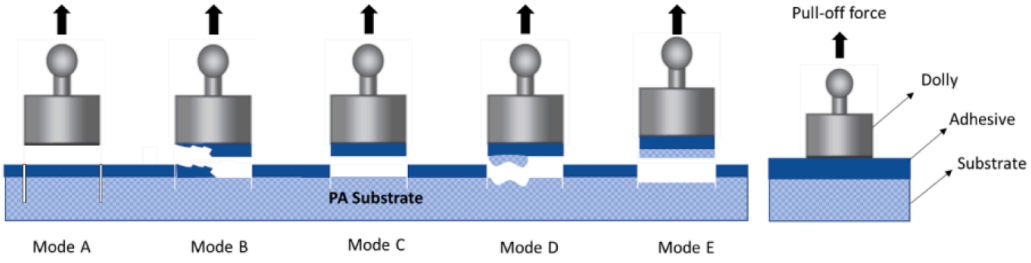


**Fig. 16.** Some of the failure modes in the pull-off test.

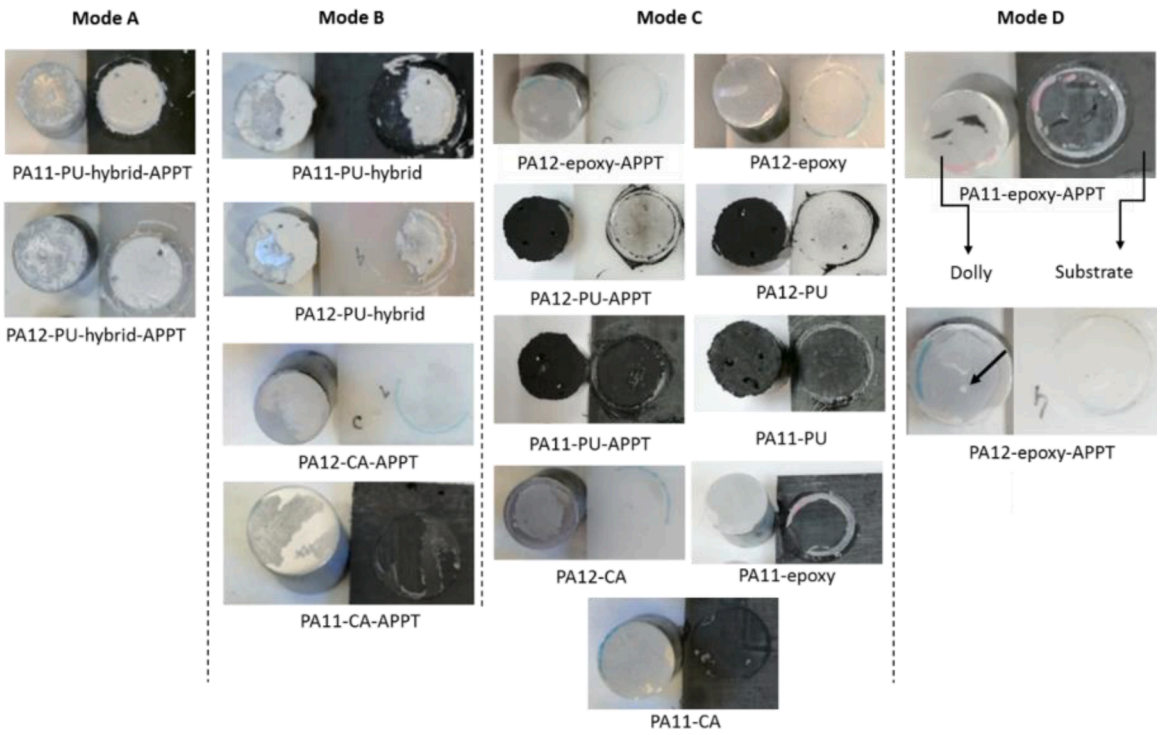


**Fig. 17.** Pulled-off samples after adhesion test for each polymer and adhesive.

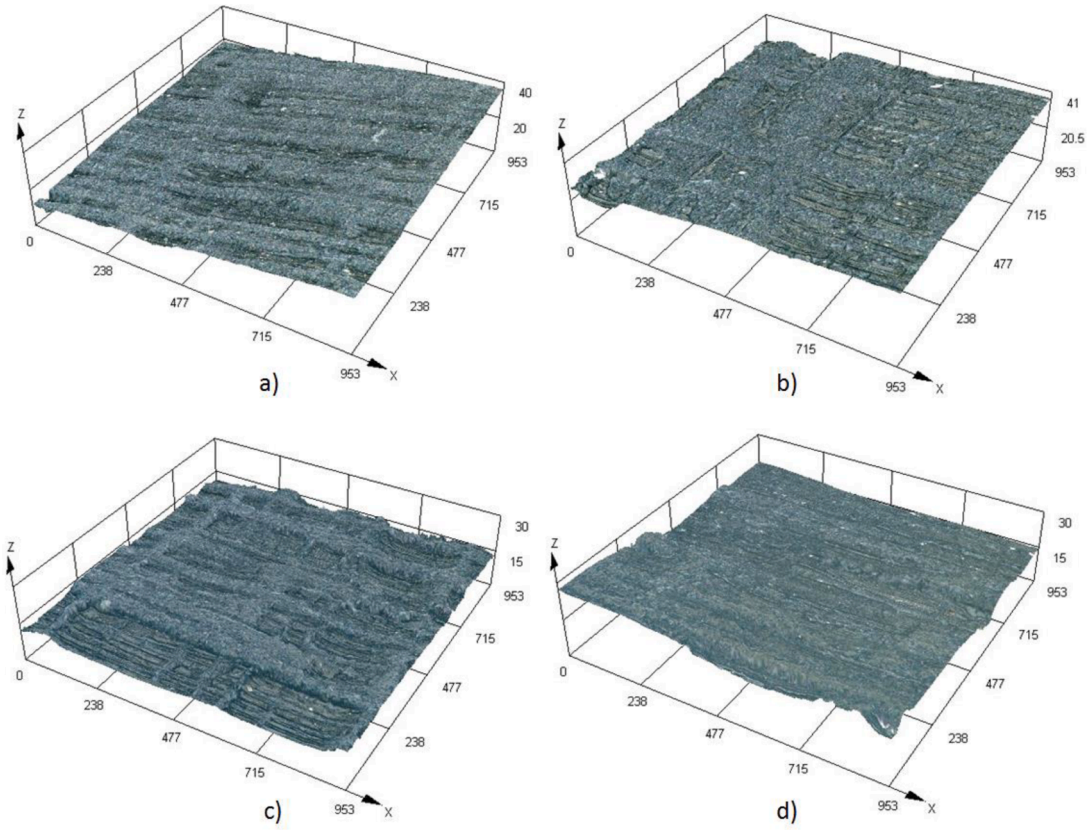


**Fig. 18.** 3D images of polyamides surfaces by CLSM: a) PA11, b) PA11-APPT, c) PA12, d) PA12-APPT.

**Table 9**
Roughness parameters of PAs before and after APPT treatment.

| Roughness parameters | PA11 | PA11-APPT | PA12 | PA12-APPT |
|---|---|---|---|---|
| $S_a$ (μm) | 0.85 | 0.56 | 0.93 | 0.67 |
| $S_{pk}$ (μm) | 0.92 | 0.71 | 1.52 | 1.12 |
| $S_k$ (μm) | 2.20 | 1.22 | 3.25 | 1.82 |
| $S_{vk}$ (μm) | 1.16 | 0.81 | 1.48 | 1.23 |
| $S_{Mr1}$ (%) | 10.19 | 12.48 | 11.98 | 13.08 |
| $S_{Mr2}$ (%) | 89.41 | 89.01 | 88.91 | 89.01 |

**Table 10**
Input values for FEM-CZM simulations and resulting fracture energy.

| Adhesive | Adhesive Strength $\sigma_{max}$ [MPa] | Stiffness for contact Kn [N/mm$^3$] | Max. crack separation $\delta_c$ [mm] | Fracture energy (bilinear CZM) [N/mm] |
|---|---|---|---|---|
| PA11 | | | | |
| Epoxy-APPT | 2.208 | 3.979 | 1 | 1.104 |
| Epoxy | 0.857 | 2.546 | 0.66 | 0.283 |
| PU-hybrid-APPT | 1.691 | 1.291 | 6 | 4.530* |
| PU-hybrid | 1.455 | 1.212 | 6.8 | 4.658* |
| PU-APPT | 1.084 | 0.546 | 6 | 2.850* |
| PU | 1.040 | 0.576 | 5 | 2.320* |
| CA-APPT | 0.539 | 0.764 | 0.65 | 0.137 |
| CA | 0.744 | 2.760 | 0.45 | 0.179 |
| PA12 | | | | |
| Epoxy-APPT | 2.628 | 4.244 | 0.7 | 0.920 |
| Epoxy | 0.672 | 0.318 | 1.75 | 0.417 |
| PU-hybrid-APPT | 1.502 | 1.205 | 6 | 4.230* |
| PU-hybrid | 1.286 | 1.222 | 5 | 3.055 |
| PU-APPT | 1.051 | 0.263 | 6.1 | 3.205* |
| PU | 0.909 | 0.455 | 6 | 2.728* |
| CA-APPT | 0.577 | 0.637 | 0.85 | 0.203 |
| CA | 0.698 | 1.702 | 0.45 | 0.134 |

* Approximated values using the bilinear CZM-law.

- The XPS and FTIR analysis results revealed that plasma generated additional oxygen-containing functional groups (C–O, C = O and O = C–N) on the surface, which reduced the hydrophobicity behavior of surfaces.
- Using DSC measurements, the neutral effect of APPT treatment on PAs' thermal properties was confirmed.
- The pull-off strength of adhesive joint to PAs was observed by a sequence of epoxy >PU-hybrid >PU >CA for both treated and untreated surfaces. In addition, APPT treatment significantly improved the adhesive bond strength of epoxy with PA11 and PA12 by 157% and 291%, respectively. On the one hand, the statistical model of ANOVA showed that APPT had no positive effect on the adhesion strength of CA, PU and PU-hybrid due to the drying effect of plasma and low surface tension energy of PUs. On the other hand, failure mode changing of CA and PU-hybrid from adhesive to cohesive failure exhibits a good substrate-adhesive bonding after APPT.
- The average micro-roughness decreased by 34% and 28% for PA11 and PA12, respectively, after APPT treatment as a result of the cleaning and ablation effect of plasma.
- The APPT treatment has a significant influence on the shape of the CZM-law for each case. In brittle adhesives, such as epoxy and cyanoacrylate, the bilinear CZM-law describes the fracture behavior adequately, and in both cases, it can reproduce the increase in strength and fracture energy. As for the elastic adhesives, a trapezoidal CZM-law would fit more adequately the experimental results, since the linear CZM-law does not fit the data adequately and requires a high computational cost to fully reproduce the test. Overall, the pull-off tests not only provide insights into the influence of the APPT treatment on the strength but also on the fracture energy and shape of the CZM-law required. This proves to be a helpful tool since the alternative tests, although standardized, require test specimens with extensive preparations.

Such results confirm the APPT treatment potential for modifying the PAs surface characterizations, which is required prior to applying adhesives or coatings to have a promising bonding.

## Authors statement

All persons who meet authorship criteria are listed as authors, and all authors certify that they have participated sufficiently in the work to take public responsibility for the content, including participation in the concept, design, analysis, writing, or revision of the manuscript. Furthermore, each author certifies that this material or similar material has not been and will not be submitted to or published in any other publication before its appearance in the *Surfaces and Interfaces*. Authorship contributions surnames, e.g., Y.L. Cheung). The name of each author must appear at least once in each of the three categories below. *Category 1* Conception and design of study: M.A. Martinez, J. Abenojar, M. Bahrami, D. Lavayen-Farfan Acquisition of data: M. Bahrami, D. Lavayen-Farfan Analysis and/or interpretation of data: M. Bahrami, D. Lavayen-Farfan, M.A. Martínez, J. Abenojar *Category 2* Drafting the manuscript: M. Bahrami, D. Lavayen-Farfan Revising the manuscript critically for important intellectual content: M. Bahrami, D. Lavayen-Farfan, M.A. Martínez, J. Abenojar *Category 3* Approval of the

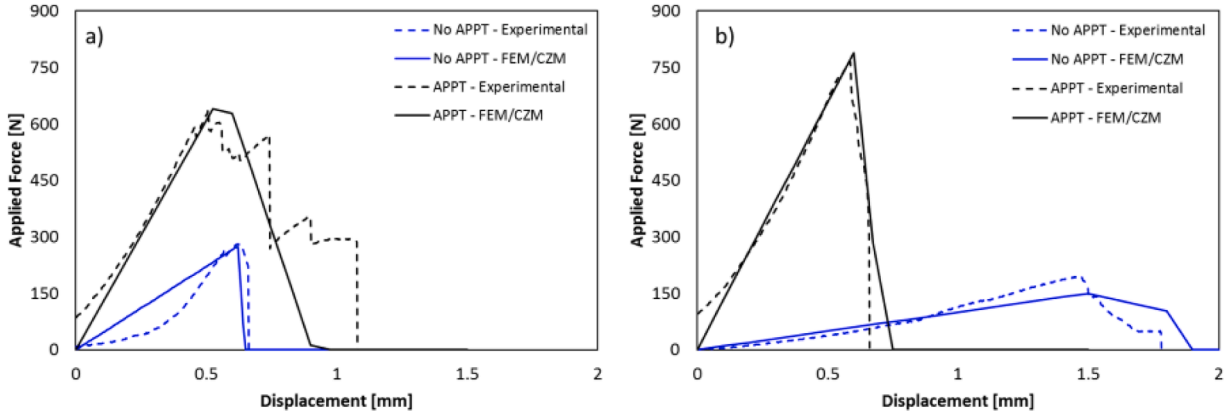


**Fig. 19.** Force – displacement curves comparison between the experimental and numerical results for the epoxy adhesive (only the average of the experimental curves is plotted to avoid cluttering): a) PA11, b) PA12.

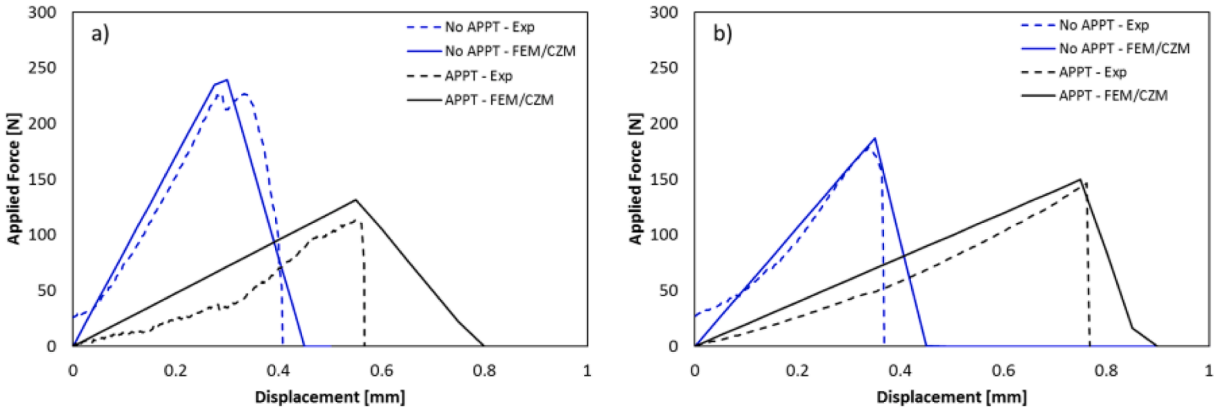


**Fig. 20.** Force – displacement curves comparison between the experimental and numerical results for the CA adhesive: a) PA11, b) PA12.

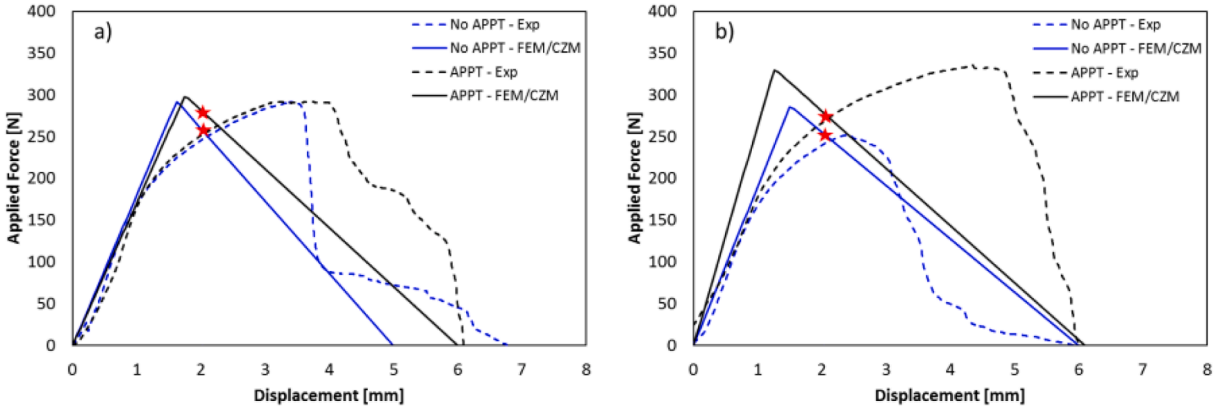


**Fig. 21.** Force – displacement curves comparison between the experimental and numerical results for the PU adhesive: a) PA11, b) PA12.

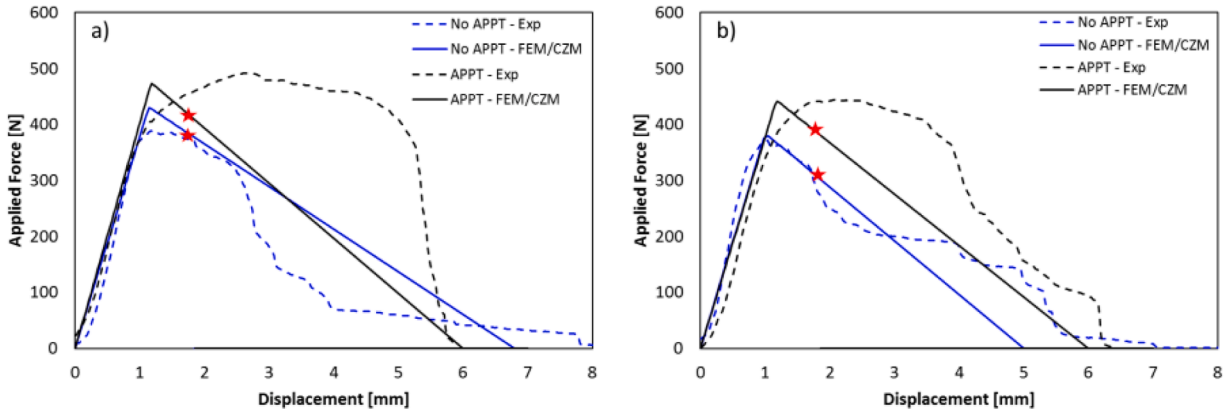


**Fig. 22.** Force – displacement curves comparison between the experimental and numerical results for the PU-hybrid adhesive: a) PA11, b) PA12.

version of the manuscript to be published (the names of all authors must be listed): M. Bahrami, D. Lavayen-Farfan, M.A. Martínez, J. Abenojar

## Authors contributions

Conceptualization and methodology: M.B., J.A., and M.Á.M.; simulation: D.L.F; writing-original draft preparation: M.B., D.L.F.; writing-review and editing: M.B., J.A., D.L.F. and M.Á.M.; supervision: J.A., and M.Á.M. All authors have read and agreed to the published version of the manuscript.

## Funding

This research did not receive any specific grant from funding agencies in the public, commercial, or not-for-profit sectors.

## Declaration of Competing Interest

The authors declare that they have no known competing financial interests or personal relationships that could have appeared to influence the work reported in this paper.

## References


[1] E.K. Bolton, Chemical Industry Medal. Development of Nylon, Indust. Engin. Chem. 34 (1) (1942) 53–58.
[2] G. Primc, Surface modification of polyamides by gaseous plasma—Review and scientific challenges, Polymers 12 (12) (2020) 3020.
[3] V. Štěpánová, et al., The effect of ambient air plasma generated by coplanar and volume dielectric barrier discharge on the surface characteristics of polyamide foils, Vacuum 183 (2021), 109887.
[4] Z. Károly, et al., Improvement of adhesion properties of polyamide 6 and polyoxymethylene-copolymer by atmospheric cold plasma treatment, Polymers 10 (12) (2018) 1380.
[5] Chemsystems Online, PERP Program – Nylon 6 and Nylon 66, N., Inc., 2009. White Plains.
[6] A. Salazar, et al., Monotonic loading and fatigue response of a bio-based polyamide PA11 and a petrol-based polyamide PA12 manufactured by selective laser sintering, Eur. Polym. J. 59 (2014) 36–45.
[7] L. Martino, et al., Bio-based polyamide 11: synthesis, rheology and solid-state properties of star structures, Eur. Polym. J. 59 (2014) 69–77.
[8] G.J. Domski, et al., Living alkene polymerization: new methods for the precision synthesis of polyolefins, Prog. Polym. Sci. 32 (1) (2007) 30–92.
[9] A.D. Mohanty, C. Bae, Transition metal-catalyzed functionalization of polyolefins containing CC, CC, and CH bonds, Adv. Organomet. Chem. 64 (2015) 1–39.
[10] A.J. Kinloch, A.J. Kinloch, Adhesion and adhesives: Science and Technology, Springer Science & Business Media, 1987.
[11] S.M. Aharoni, n-Nylons: Their synthesis, structure, and Properties, Wiley-Blackwell, 1997.
[12] J. Kim, H.-s. Kim, C.H. Park, Contribution of surface energy and roughness to the wettability of polyamide 6 and polypropylene film in the plasma-induced process, Text. Res. J. 86 (5) (2016) 461–471.
[13] I. Novák, M. Števiar, I. Chodák, Surface energy and adhesive properties of polyamide 12 modified by barrier and radio-frequency discharge plasma, Monatshefte für Chemie/Chemical Monthly 137 (7) (2006) 943–952.
[14] M. Hutchins, G. Smyrna, Adhesion to Plastic, RadTech e, 2006.
[15] F. Awaja, et al., Adhesion of polymers, Prog. Polym. Sci. 34 (9) (2009) 948–968.
[16] Z. Károly, et al., Effect of atmospheric cold plasma treatment on the adhesion and tribological properties of polyamide 66 and poly (tetrafluoroethylene), Materials 12 (4) (2019) 658.
[17] C. Mandolfino, E. Lertora, C. Gambaro, Influence of cold plasma treatment parameters on the mechanical properties of polyamide homogeneous bonded joints, Surf. Coat. Technol. 313 (2017) 222–229.
[18] J. Hnilica, et al., Rapid surface treatment of polyamide 12 by microwave plasma jet, Appl. Surf. Sci. 288 (2014) 251–257.
[19] Z. Gao, et al., Surface modification of a polyamide 6 film by He/CF4 plasma using atmospheric pressure plasma jet, Appl. Surf. Sci. 256 (5) (2009) 1496–1501.
[20] Z. Gao, et al., The influence of moisture on atmospheric pressure plasma etching of PA6 films, Curr. Appl Phys. 10 (1) (2010) 230–234.
[21] Z. Gao, et al., Influence of processing parameters on atmospheric pressure plasma etching of polyamide 6 films, Appl. Surf. Sci. 255 (17) (2009) 7683–7688.
[22] Z. Gao, Influence of environmental humidity on plasma etching polyamide 6 films, Appl. Surf. Sci. 258 (15) (2012) 5574–5578.
[23] C. Lambare, et al., Plasma functionalization and etching for enhancing metal adhesion onto polymeric substrates, RSC Adv. 5 (77) (2015) 62348–62357.
[24] N. Encinas, et al., Atmospheric pressure plasma hydrophilic modification of a silicone surface, J. Adhesion 88 (4-6) (2012) 321–336.
[25] M. Bahrami, et al., Characterization of hybrid biocomposite Poly-Butyl-Succinate/Carbon fibers/Flax fibers, Engineering (2021), 109033.
[26] M.A. Martinez, J. Abenojar, S. Lopez de Armentia, Environmentally friendly plasma activation of acrylonitrile–butadiene–styrene and polydimethylsiloxane surfaces to improve paint adhesion, Coatings 8 (12) (2018) 428.
[27] M.A. Martinez, et al., Effect of atmospheric plasma torch on ballistic woven aramid, Text. Res. J. 87 (19) (2017) 2358–2367.
[28] S.L. de Armentia, et al., Novel application of a thermoplastic composite with improved matrix-fiber interface, J. Mater. Res. Technol. 8 (6) (2019) 5536–5547.
[29] D.S. Dugdale, Yielding of steel sheets containing slits, J. Mech. Phys. Solids 8 (2) (1960) 100–104.
[30] G.I. Barenblatt, The mathematical theory of equilibrium cracks in brittle fracture. Advances in Applied Mechanics, Elsevier, 1962, pp. 55–129.
[31] L. Jiang, et al., Estimating the cohesive zone model parameters of carbon nanotube–polymer interface for machining simulations, J. Manuf. Sci. Eng. 136 (3) (2014).
[32] R. Ghandriz, K. Hart, J. Li, Extended finite element method (XFEM) modeling of fracture in additively manufactured polymers, Additive Manufact. 31 (2020), 100945.
[33] T. Yang, K.M. Liechti, R. Huang, A multiscale cohesive zone model for rate-dependent fracture of interfaces, J. Mech. Phys. Solids 145 (2020), 104142.
[34] K. Pandya, J. Williams, Cohesive zone modelling of crack growth in polymers part 1–experimental measurement of cohesive law, Plast. Rubber Compos. 29 (9) (2000) 439–446.
[35] Normalización, O.I.d., Adhesives: Determination of the Mode 1 Adhesive Fracture Energy of Structural Adhesive Joints Using Double Cantilever Beam and Tapered Double Cantilever Beam Specimens, ISO, 2009.
[36] J. Zhang, et al., Effect of the cohesive law shape on the modelling of adhesive joints bonded with brittle and ductile adhesives, Int. J. Adhes. Adhes. 85 (2018) 37–43.
[37] R. Lopes, et al., Comparative evaluation of the double-cantilever beam and tapered double-cantilever beam tests for estimation of the tensile fracture toughness of adhesive joints, Int. J. Adhes. Adhes. 67 (2016) 103–111.
[38] R.D. Campilho, et al., Modelling adhesive joints with cohesive zone models: effect of the cohesive law shape of the adhesive layer, Int. J. Adhes. Adhes. 44 (2013) 48–56.
[39] L. Škec, G. Alfano, G. Jelenić, On Gc, Jc and the characterisation of the mode-I fracture resistance in delamination or adhesive debonding, Int. J. Solids Struct. 144 (2018) 100–122.
[40] L. Škec, G. Alfano, G. Jelenić, Enhanced simple beam theory for characterising mode-I fracture resistance via a double cantilever beam test, Engineering 167 (2019) 250–262.
[41] M. Bahrami, J. Abenojar, M.A. Martínez, Comparative Characterization of Hot-Pressed Polyamide 11 and 12: mechanical, Thermal and Durability Properties, Polymers 13 (20) (2021) 3553.
[42] J. Abenojar, et al., Thermal characterization and diffusivity of two mono-component epoxies for transformer insulation, Int. J. Adhes. Adhes. 103 (2020), 102726.
[43] P. Galvez, J. Abenojar, M.A. Martinez, Durability of steel-CFRP structural adhesive joints with polyurethane adhesives, Engineering 165 (2019) 1–9.
[44] W.F. Thomsen, *Cyanoacrylate Adhesives*, in *Adhesives in Manufacturing*, Routledge, 1983, pp. 305–323.
[45] D. Owens, Some thermodynamic aspects of polymer adhesion, J. Appl. Polym. Sci. 14 (7) (1970) 1725–1730.
[46] N. Selvakumar, H.C. Barshilia, K. Rajam, Effect of substrate roughness on the apparent surface free energy of sputter deposited superhydrophobic polytetrafluoroethylene coatings: a comparison of experimental data with different theoretical models, J. Appl. Phys. 108 (1) (2010), 013505.
[47] D.K. Owens, R. Wendt, Estimation of the surface free energy of polymers, J. Appl. Polym. Sci. 13 (8) (1969) 1741–1747.
[48] J. Krizbergs, A. Kromanis, Methods for prediction of the surface roughness 3D parameters according to technological parameters, in: 5th International DAAM Baltic Conference,, Industrial engineering-adding innovation capacity of labour force and entrepreneurs'', Tallinn, Estonia, 2006.
[49] W. Dong, P. Sullivan, K. Stout, Comprehensive study of parameters for characterising three-dimensional surface topography: III: parameters for characterising amplitude and some functional properties, Wear 178 (1-2) (1994) 29–43.
[50] ISO-13565-2, B.S.I., Geometric product specifications (gps) surface texture: profile method, surfaces having stratified functional propertie, Height Characteriz. Using Linear Mater. Ration Curve (1997).
[51] S. Ebnesajjad, C. Ebnesajjad, Surface Treatment of Materials For Adhesive Bonding, 2nd ed., William Andrew, 2013.
[52] M. Tatoulian, et al., Role of helium plasma pretreatment in the stability of the wettability, adhesion, and mechanical properties of ammonia plasma-treated polymers. Application to the Al-polypropylene system, J. Adhes. Sci. Technol. 9 (7) (1995) 923–934.
[53] F. Ippolito, et al., Calcium Carbonate as Functional Filler in Polyamide 12-Manipulation of the Thermal and Mechanical Properties, Processes 9 (6) (2021) 937.
[54] E. Ogunsona, et al., A critical review on the fabrication processes and performance of polyamide biocomposites from a biofiller perspective, Mater. Today Sustain. 5 (2019), 100014.
[55] M. Nikforooz, et al., Processability and tensile performance of continuous glass fiber/polyamide laminates for structural load-bearing applications, Composites, Part A 105 (2018) 156–164.
[56] G. Socrates, Infrared and Raman characteristic Group frequencies: Tables and Charts, 3rd ed., John Wiley & Sons, 2004.
[57] P. Kuang, K. Constant, M. Aliofkhazraei, Increased wettability and surface free energy of polyurethane by ultraviolet ozone treatment, in: M. Aliofkhazraei (Ed.), Wetting and Wettability, InTech, 2015, pp. 85–104. Editor.
[58] ASTM-D7522, Standard Test Method For Pull-Off Strength For FRP Bonded to Concrete Substrate, ASTM International, West Conshohocken, PA, 2009.
[59] J. Hsieh, C. Li, Effects of hollow cathode and Ar/H2 ratio on plasma cleaning of Cu leadframe, Thin. Solid. Films 504 (1-2) (2006) 101–103.
[60] J. Hsieh, et al., Plasma cleaning of copper leadframe with Ar and Ar/H2 gases, Surf. Coat. Technol. 112 (1-3) (1999) 245–249.
[61] P.S. Arinda, et al., Stability of polystyrene film surface wettability modified using oxygen plasma, Mater. Today: Proc. 13 (2019) 24–29.
[62] J. Siegel, et al., Ablation and water etching of plasma-treated polymers, Radiat. Effects Defects Solids 163 (9) (2008) 779–788.
[63] C. Cardinaud, M.-.C. Peignon, P.-.Y. Tessier, Plasma etching: principles, mechanisms, application to micro-and nano-technologies, Appl. Surf. Sci. 164 (1-4) (2000) 72–83.
[64] R.M. Sanchis, et al., Enhancement of wettability in low density polyethylene films using low pressure glow discharge N2 plasma, J. Polym. Sci. Part B Polym. Phys. 45 (17) (2007) 2390–2399.